

Zero-Permutation Jet-Parton Assignment using a Self-Attention Network

Jason Sang Hun Lee, Inkyu Park, Ian James Watson, and Seungjin Yang

Department of Physics, University of Seoul, Seoul 02504, Republic of Korea

*E-mail: jlee@physics.uos.ac.kr, icpark@physics.uos.ac.kr,
ijwatson@physics.uos.ac.kr, seungjin.yang@physics.uos.ac.kr*

ABSTRACT:

In high-energy particle physics events, it can be advantageous to find the jets associated to the decays of intermediate states, for example the three jets produced by the hadronic decay of the top quark. Typically, a goodness-of-association measure, such as a χ^2 related to the mass of the associated jets, is constructed, and the best jet combination is found by optimising this measure. As this process suffers from combinatorial explosion with the number of jets, the number of permutations is limited by using only the n highest p_T jets. The self-attention block is a neural network unit used for the neural machine translation problem, which can highlight relationships between any number of inputs in a single iteration without permutations. In this paper, we introduce the [Self-Attention for Jet Assignment \(SAJA\) network](#). SAJA can take any number of jets for input, and outputs probabilities of jet-parton assignment for all jets in a single step. We apply SAJA to find jet-parton assignments of fully-hadronic $t\bar{t}$ events to evaluate the performance. We show that SAJA achieves better performance than a likelihood based approach, while providing a lower latency that is nearly constant regardless of the number of input jets.

Contents

1	Introduction	1
2	SAJA network	2
2.1	Objective function	2
2.2	Self-attention	3
2.3	Architecture	4
2.4	Predictive uncertainty	5
3	Monte Carlo Samples and Event Selection	6
3.1	Dataset	7
3.2	Training	9
4	Results	9
4.1	Performance	9
4.2	Predictive Entropy	11
4.3	Model Interpretability	14
4.4	Latency	14
5	Conclusions	15

1 Introduction

The final state of proton–proton collisions is an explosion of particles. To tame the complexity of the description of the collision, we can order the particles by clustering them into jets, final state collections of particles which are produced from an underlying parton produced in the hard interaction. In events which are assumed to be produced from heavy intermediate particles, such as the top quark, which can decay into three partons, it can be useful to further find the jets correlated with the decay of the underlying top parton. Typically, a goodness-of-association measure, such as a χ^2 or likelihood related to the mass of the associated jets, is constructed, and jet combinations are tried in turn to find the combination with the minimal χ^2 which is used as the assignment for further analysis [1–3]. This process suffers from combinatorial explosion as the number of jets can get quite high and usually only combinations of the n highest p_T jets are tried, where n is usually restricted to at most six or seven. Recently, machine learning algorithms such as boosted decision trees and fully-connected neural networks have also been used to learn a goodness-of-association measure for jet-parton assignment [4, 5]. However, while these approaches show better performance than existing kinematic fitting method, they still suffer from the problem of combinatorial explosion as they also operate on individual permutations of the jets.

Recent advances in deep neural networks have led us to a solution which analogizes the jet-parton association problem to finding connections between words in a sentence, and how words in the sentence are translated to another language [6–9]. As languages do not map one-to-one, words corresponding to different concepts can appear at different points in the sentence and its translation. In our case, the source language corresponds to the reconstructed jets and the target language is the parton assignment for each jet. The self-attention block is a neural network unit used in the machine translation problem, which can highlight relationships between any number of inputs in a single step.

In this paper, we introduce the Self-Attention for Jet Assignment (SAJA) network. As the name implies, it uses self-attention blocks to find the relationships between jets in the event. SAJA can take any number of jets for input, and outputs the probability of association to the possible jet-parton assignment categories for all jets. In section 2 we describe the SAJA network and the produces we use to optimize the network. The performance of SAJA is tested on fully-hadronic $t\bar{t}$ events. Fully-hadronic $t\bar{t}$ is one of the standard model decay modes with the most number of jets, which makes the traditional iterative methods limited due to the exponential permutations. In section 3 we describe this dataset and the analysis procedure. Finally, in section 4, we show the results of applying SAJA to the all-hadronic top pair channel, and compare the performance with a likelihood-based approach.

2 SAJA network

2.1 Objective function

We consider the jet-parton assignment problem as a jet-wise multi-class classification task. That is, we will build a model which, for each jet in the event, gives a probability for the jet to belong to each of several classes. For our example of fully hadronically decaying top pair production, there are five classes: b-jets produced in the decay $t \rightarrow bW$, light quark jets from the decay $W \rightarrow jj'$, b-jets and W jets produced from the equivalent anti-top decays, and jets not associated to the top quark decays, which we will call other jets. Since it is hard to distinguish jets originating from t and jets originating from \bar{t} when both tops are hadronically decaying, we introduce arbitrary indices 1 and 2 for either of the top-quark pair and their decay products, and develop an objective function which is insensitive to the ordering of the jets.

The model is thus a function f^θ of the form:

$$f^\theta : \begin{pmatrix} \mathbf{x}^{(1)} \\ \vdots \\ \mathbf{x}^{(N)} \end{pmatrix} \rightarrow \begin{pmatrix} \hat{y}_{b_1}^{(1)} & \hat{y}_{W_1}^{(1)} & \hat{y}_{b_2}^{(1)} & \hat{y}_{W_2}^{(1)} & \hat{y}_{\text{other}}^{(1)} \\ \vdots & \vdots & \vdots & \vdots & \vdots \\ \hat{y}_{b_1}^{(N)} & \hat{y}_{W_1}^{(N)} & \hat{y}_{b_2}^{(N)} & \hat{y}_{W_2}^{(N)} & \hat{y}_{\text{other}}^{(N)} \end{pmatrix} \quad (2.1)$$

where $\mathbf{x}^{(j)}$ indicates the jet in the event with index j and $\hat{y}_{\text{class}}^{(j)}$ indicates the probability for jet i to belong to the category class and the corresponding truth label will be denoted $y_{\text{class}}^{(j)}$ which is 1 if the jet has been matched to the class and 0 otherwise.

Since our task is the jet-wise classification, we can use jet-wise cross-entropy as the objective function. Since our indices are arbitrary, there remains an ambiguity by permuting t and \bar{t} between indices 1 and 2. Therefore, we write the objective function as:

$$J(\theta) = \frac{1}{N} \sum_{j=1}^N [\min(\pi_{12}^{(j)}, \pi_{21}^{(j)}) + y_{\text{other}}^{(j)} \log \hat{y}_{\text{other}}^{(j)}], \quad (2.2)$$

where $\pi_{\alpha\beta}^{(j)} = y_b^{(j)} \log \hat{y}_{b_\alpha}^{(j)} + y_{\bar{b}}^{(j)} \log \hat{y}_{b_\beta}^{(j)} + y_{W^+}^{(j)} \log \hat{y}_{W_\alpha}^{(j)} + y_{W^-}^{(j)} \log \hat{y}_{W_\beta}^{(j)}$ with $\alpha, \beta \in 1, 2$. Since the min function is invariant under the permutation of arguments, Eq. 2.2 is independent of the top or anti-top being assigned to the first or second top.

2.2 Self-attention

Self-attention is a special case of the more general attention mechanism, of which there are several implementations such as additive attention [6] and dot-product attention [8]. In this paper, we use the scaled dot-product attention which was introduced in the Transformer network [9]. The scaled dot-product attention is a function that takes three sets of vectors as inputs and produces a single output set. In the original Transformer paper, inputs are called sentences in the context of the natural language processing. However, the scaled dot-product attention is invariant under the permutation of elements. Therefore, we refer to the input of the attention block as a ‘set’. For example, a sentence is a set of words, each of which is represented as a vector using the word embedding. Another example of an input set is an image, which is a set of pixels that are vectors of RGB values.

The three input sets of the attention block are called keys, values and queries, which are denoted by K , V and Q respectively. The cardinalities of K and V are required to be the same and will be denoted S , while Q may differ and will be denoted T . A set is represented as a matrix, where each row is a vector of the set. In general, the key set and the value set are derived from a single set called the source, the jet inputs in our case. The source set is transformed into a key and value set using two different element-wise linear transformations. Self-attention is the special case where the query set is also derived from the source set in the same manner. In summary, the sets derived from the source set are:

$$K = \begin{pmatrix} \vec{k}^{(1)} \\ \vdots \\ \vec{k}^{(S)} \end{pmatrix} = \begin{pmatrix} W_K \vec{x}^{(1)} \\ \vdots \\ W_K \vec{x}^{(S)} \end{pmatrix}, \quad V = \begin{pmatrix} \vec{v}^{(1)} \\ \vdots \\ \vec{v}^{(S)} \end{pmatrix} = \begin{pmatrix} W_V \vec{x}^{(1)} \\ \vdots \\ W_V \vec{x}^{(S)} \end{pmatrix}, \quad \text{and} \quad Q = \begin{pmatrix} \vec{q}^{(1)} \\ \vdots \\ \vec{q}^{(T)} \end{pmatrix} = \begin{pmatrix} W_Q \vec{x}^{(1)} \\ \vdots \\ W_Q \vec{x}^{(T)} \end{pmatrix}, \quad (2.3)$$

where $\vec{x}^{(k)}$ is a vector of the source set, W_K , W_V , W_Q are linear transformation matrices and $\dim \vec{k}^{(i)} = \dim \vec{q}^{(j)}$ for all i and j . To form the Attention layer, first Q and K are matrix multiplied and then scaled by the dimension of a key vector d_k to form the matrix E . Then the softmax function is applied to each row of E and the elements of the resulting matrix A called the attention weights.

$$A_{ij} = \frac{e^{E_{ij}}}{Z_i}, \quad \text{where} \quad E_{ij} = \frac{1}{\sqrt{d_k}} \vec{q}^{(i)} \cdot \vec{k}^{(j)} \quad \text{and} \quad Z_i = \sum_{j=1}^N e^{E_{ij}} \quad (2.4)$$

If the scaling isn't applied into 2.4, the magnitude of E_{ij} increase as d_k increases. If E_{ij} increases, the gradient of A_{ij} goes to zero. Thus, the scaling in 2.4 is a simple remedy for vanishing gradient.

Finally, attention weights are multiplied by the values v to get the output of the self-attention layer H_i .

$$H_i = \sum_{j=1}^T A_{ij} \vec{v}^{(j)} \quad (2.5)$$

Therefore, the self-attention layer is a weighted sum of the elements of the input set and is insensitive to the ordering of elements.

In real world usage, multiple attention functions are computed in parallel to increase the representation power. The multi-head attention mechanism has multiple branches (called heads), where the above self-attention is performed for each head separately on the input, resulting in multiple H_i outputs. These outputs are concatenated into a single matrix along the feature axis, then a final element-wise linear transformation is applied, resulting in the output of the multi-head attention layer.

2.3 Architecture

The architecture of SAJA, which was inspired by the encoder of the Transformer, and its two building blocks are shown in figure 1. The two building blocks are the jet-wise feed-forward network and the multi-head self-attention block. The multi-head self-attention block also includes the feed-forward network again. The feed-forward network consists of an affine transformation, a leaky ReLU [22], a dropout [23], and an affine transformation followed by a leaky ReLU. The multi-head self-attention block consists of the multi-head self-attention layer and the feed-forward network, each of which is sandwiched between layer normalization [24] and dropout, and has skip connection [25].

At the bottom of SAJA, a feed-forward layer takes a set of vectors (jets) as the input. The first affine transformation layer produces vectors with dimension of d_{FFN} and the second one produces vectors with dimension of d_{model} . The output of the bottom feed-forward network is passed through a stack of N_{block} multi-head self-attention blocks, each of which has N_{head} heads. A top feed-forward layer followed by jet-wise softmax takes the output of a last multi-head self-attention layer and then produces the assignment score. The dimension of the first affine transformation output is d_{FFN} and the second one is 5, which corresponds the number of classes. Therefore, with this setup, the hyperparameters of SAJA are only d_{model} , d_{FFN} , N_{block} , and N_{head} , where $d_{\text{model}} = d_k \times N_{\text{head}}$.

All operations, except for the self-attention are jet-wise and the self-attention, are invariant under jet permutations, resulting in SAJA being invariant under jet permutations. This property can be used to open the black-box of SAJA with Monte Carlo information, by ordering the inputs by the truth labels without affecting the resulting output. The two main operations of SAJA are affine transformations and the attention function. They both consist of matrix multiplications, which can be computed through highly optimized routines and accelerated by GPUs.

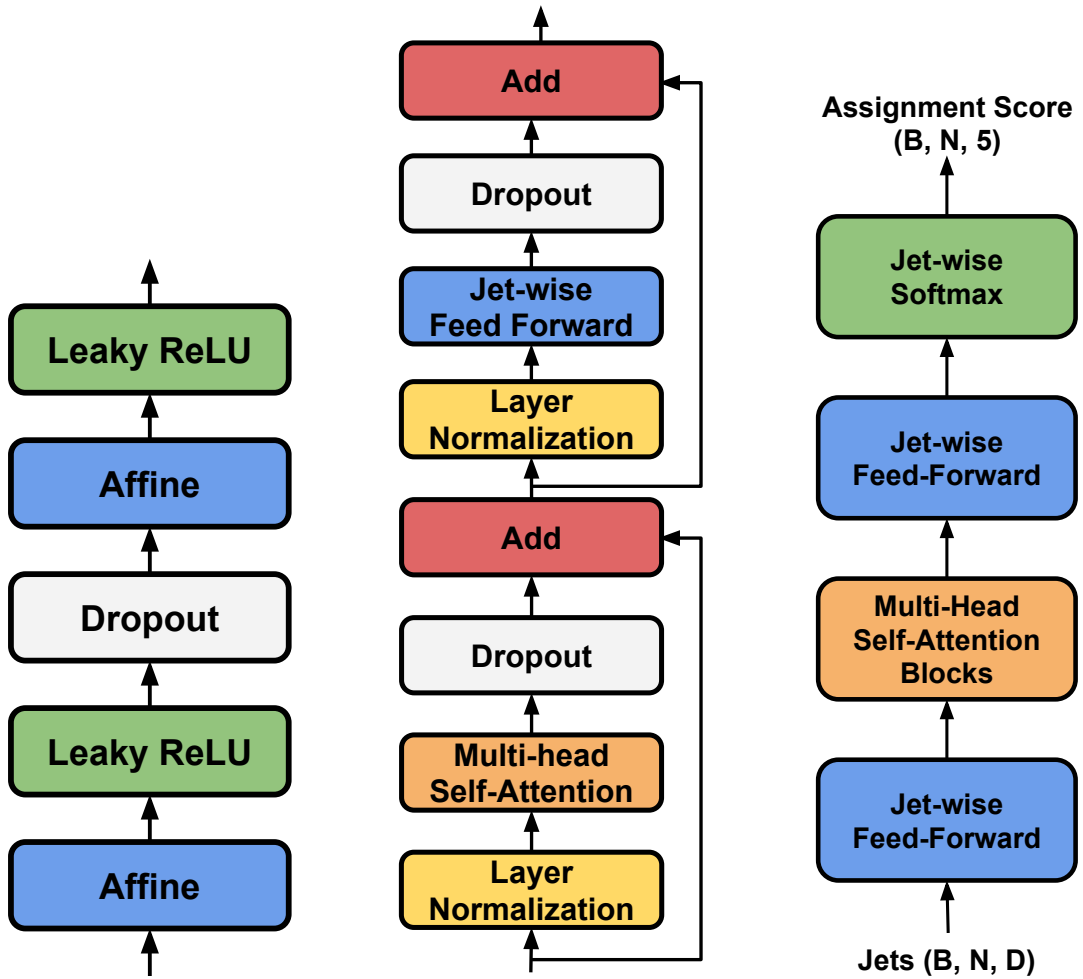


Figure 1: Jet-wise feed-forward network (left), multi-head self-attention block (center), and SAJA (right). B denotes the size of batch. N indicates the maximum number of jets in the batch. D indicates the number of features representing the jet.

2.4 Predictive uncertainty

Uncertainty quantification in deep learning is becoming more important as deep learning is applied to the real world [10]. Poor predictions by deep learning model can pose danger, especially when deep learning is being deployed in situations such as for self-driving cars and medical diagnosis. Models can also be presented with out-of-distribution (OOD) data, which is data that does not follow the distribution of the training set data. In these cases, an uncertainty estimate can be used to override a decision made by the AI. Similarly, SAJA can make wrong assignments in fully hadronic $t\bar{t}$ events, resulting in poor resolution of the kinematics of the reconstructed top quark. SAJA will also be exposed to background events such as QCD multijet during the inference (physics analysis) phase. Therefore, we will use deep learning uncertainty in order to veto both poor jet-parton assignments on fully hadronic $t\bar{t}$ events and background events.

There are various types of uncertainties that have been proposed for deep learning models [11], from which we will use the predictive entropy. As SAJA does not make a prediction for a single object, it simultaneously predicts the class of all jets in the event, we use the average of the jet-wise predictive entropy, $H[\hat{Y}]$:

$$H[\hat{Y}] = \frac{1}{N} \sum_{j=1}^N \left(- \sum_{c \in \text{classes}} \hat{y}_c^{(j)} \log \hat{y}_c^{(j)} \right) \quad (2.6)$$

We will use this predictive entropy as an event selection, when the jet-parton assignment results in a predictive entropy higher than the threshold, which means the network has given an uncertain assignment for all the jets in the event, the event is rejected.

One of the most promising application of the deep learning uncertainty is to detect OOD test data. In this study, QCD multijet background events exactly correspond to an OOD sample. In many case, the prediction score of modern deep learning classifiers are not calibrated and can classify OOD data as an in-distribution class with high confidence [12]. However, SAJA, shows reasonable uncertainty distributions for all physics process without any calibration method, as will be shown in section 4.

3 Monte Carlo Samples and Event Selection

We simulate all-hadronic $t\bar{t}$ pair production with up to two additional jets in the final state from pp collisions at $\sqrt{s} = 13$ TeV using `MADGRAPH5_AMC@NLO` v2.2.2 at next to leading order [13]. For the event generation, the top quark mass is set to 172.5 GeV. We also generate QCD events using `MADGRAPH_AMC@NLO` at leading order with two to four partons in the final state, which are the main background for the all-hadronic $t\bar{t}$ event analysis. The hard process events are interfaced to `PYTHIA 8.212` which simulates the parton shower and hadronization [14]. The hadronized events are then processed by `DELPHES v3.4.2` [15], which performs a fast detector response simulation and particle-flow event reconstruction for a CMS-like detector and uses `FASTJET 3.3.2` to perform anti- k_T jet clustering [16]. The jet-clustering parameter R is modified, from the default CMS card provided with the `DELPHES` package, from 0.5 to 0.4 to match the value that CMS uses for 13 TeV data.

We also generate $t\bar{t}$ events using `POWHEGv2` [17–20] interfaced to both `PYTHIA8.212` and `HERWIG++ 2.7.1` [21] to check for Monte Carlo dependency of our results. To match the matrix element and parton shower, we use h_{damp} values of 1.581 for `PYTHIA8` and 1 for `HERWIG++`.

We follow the trigger selection used in the CMS all-hadronic top pair analysis to select events for further study [1]. We use jets with $p_T > 30$ GeV and $|\eta| < 2.4$. We select events which contain at least 6 jets with $p_T > 40$ GeV, at least one of which is b-tagged. We then require $H_T = \sum_{\text{jets}} p_T > 450$ GeV.

We generated about 19.4 million $t\bar{t}$ events using `MADGRAPH5_AMC@NLO` with `PYTHIA8`, of which about 2.4 million events passed the event selection. We generated QCD in seven H_T bins to increase the event statistics at high H_T . In total, 157.5 million QCD events were generated, of which 1.1 million passed the event selection.

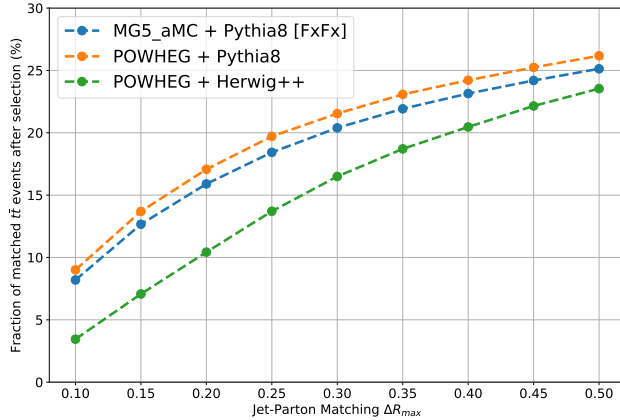


Figure 2: Fraction of matched $t\bar{t}$ events after the event selection vs. angular distance threshold between a parton and a jet $\Delta R_{max}(\text{jet, parton})$. MADGRAPH_AMC@NLO interfaced to PYTHIA8 (blue), POWHEG interfaced to PYTHIA8 (orange), and POWHEG interfaced to HERWIG++ (green). MADGRAPH_AMC@NLO interfaced to PYTHIA8 with $\Delta R_{max} = 0.3$ events are used for training.

In order to study the performance of the jet-parton assignment, we match the reconstructed jets to the outgoing partons of the matrix elements. We perform a geometric matching between jets and partons in $\eta - \phi$ space requiring matched jets and partons to be separated by less than 0.3 in ΔR and by pairing a jet and a parton at the nearest distance first, and removing both from the list of potential matches. Figure 2 shows the fraction of matched $t\bar{t}$ events as a function of $\Delta R(\text{jet, parton})$ for the three event generators. POWHEG v2 with PYTHIA8 has the fraction about 1% higher than MADGRAPH5_AMC@NLO with PYTHIA8. The difference between POWHEG v2 with HERWIG++ and MADGRAPH5_AMC@NLO with PYTHIA8 decrease from about 5.6% to 1.6% as ΔR increases. The proportion of selected top pair events where all partons are matched is about 20%. We call top pair events where the jet-parton matching failed to match all the partons unmatched events and consider them background for the purpose of this study.

The jet multiplicity distributions for matched $t\bar{t}$ events are shown in figure 3. Figure 4 shows the fraction of matched $t\bar{t}$ events, where all partons can be matched with the most energetic N jets without considering b-tag information. These numbers can be interpreted as the naive upper limit of the performance of a jet-parton assignment model that takes most energetic N jets.

3.1 Dataset

All jets in the event are used as input to the SAJA network. Jets are inputs into the network using high level reconstructed variables. These are the jet p_T , η , ϕ , $\frac{p_T}{H_T}$, and whether the jet is b-tagged.

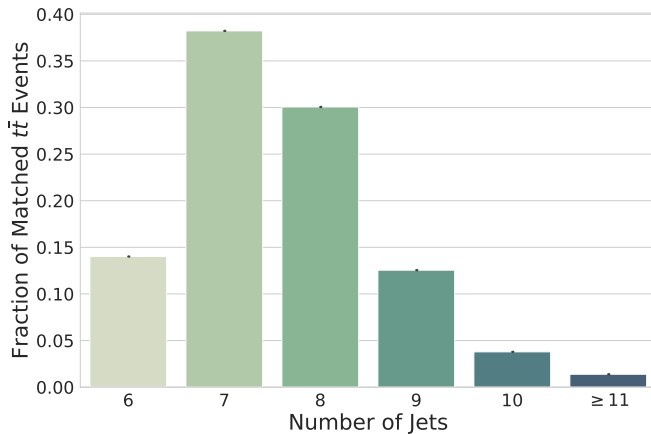


Figure 3: The jet multiplicity distribution for matched $t\bar{t}$

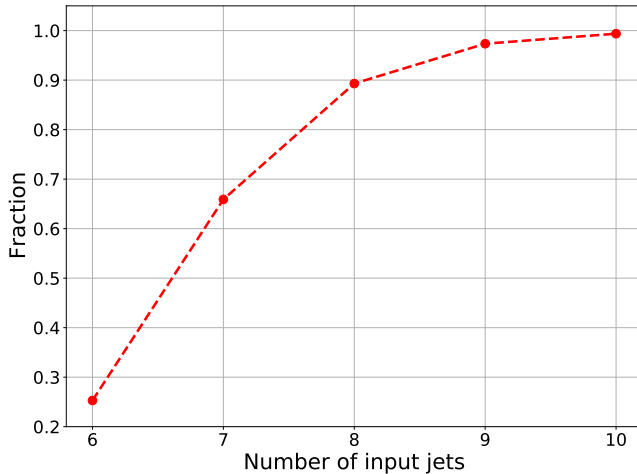


Figure 4: The fraction of matched $t\bar{t}$ events, where all partons can be matched with most energetic N jets without considering b-tag information.

We also tested the impact of using additional jet shape variables. Gluon-initiated jets should always be assigned to “other” class, and these variables can be helpful to distinguish quark from gluon jets. We used eight variables, which are the simple extension of three quark-gluon discrimination variables used by CMS [26] and shown to be effective in quark-gluon separation [27]. The variables are the jet energy sharing variables, major and minor axes of the jet in $\eta - \phi$ space, and the multiplicity of each particle flow type. All features except b-tag are scaled to the range from 0 to 1 using Min-Max scaling in order to stabilize the optimization process.

Hyperparameters	SAJA without Jet Shape	SAJA with Jet Shape
d_k	16	32
N_{head}	10	10
d_{FFN}	1024	1024
N_{block}	6	6

Table 1: Hyperparameters of SAJA with and without jet shape.

3.2 Training

We used the Adam optimization algorithm [28] to minimize the objective function given in equation 2.2 and reduced the learning rate by the factor of 2 when the loss on the validation dataset did not decrease over 10 epochs. A batch size of 512 is used during the training. PYTORCH v.1.4.0 is used for implementation [29]. We used 310k, 80k and 100k matched $t\bar{t}$ for training, validation and test, respectively. The hyperparameters were optimized by hand as the search space is quite small. The hyperparameters used for this study are listed in Table 1.

We also used a kinematic likelihood fit to do jet-parton assignment to compare the performance of SAJA. We used the KLFITTER library to perform the kinematic likelihood fitting [3]. For the fit, the invariant mass of W boson is fixed to $m_W = 80.4$ GeV, while the top quark invariant mass was floated in the fit. We derived the transfer functions required by KLFitter from our top pair dataset. The transfer function is modelled by a Crystal Ball function, whose parameters are parameterized by the energy of the matching parton with separate parameterizations for barrel and endcap jets.

As more jets are used, the number of permutations increases exponentially, and therefore, we could not use all the jets in an event to study the KLFitter performance. We studied two different cases of jet inputs. In the first case, the 6 most energetic jets in the event were used as inputs to the fit, which gives a total of 18 permutations. In the second case, when more than 6 jets were in the event, we tried permutations of the 7 most energetic jets, giving an average of 126 permutations for the dataset. The permutation with the lowest likelihood after fitting was taken as the jet-parton assignment for the event. The value of the likelihood was also used as a goodness-of-fit measure. When the best permutation has a likelihood lower than a threshold, the event is rejected.

4 Results

4.1 Performance

Jet-parton assignments are used to reconstruct the signal topology but can also be useful to reject background events, by checking the topological compatibility. Therefore, in this study, we measure not only the fraction of correct assignment for the matched $t\bar{t}$ events but also the rejection rates for unmatched $t\bar{t}$ and QCD multijet.

Figure 5 show ROC-like curves, where the fraction of wrong assignments for matched $t\bar{t}$ and the rejection rate for background events as a function of correct assignments for matched

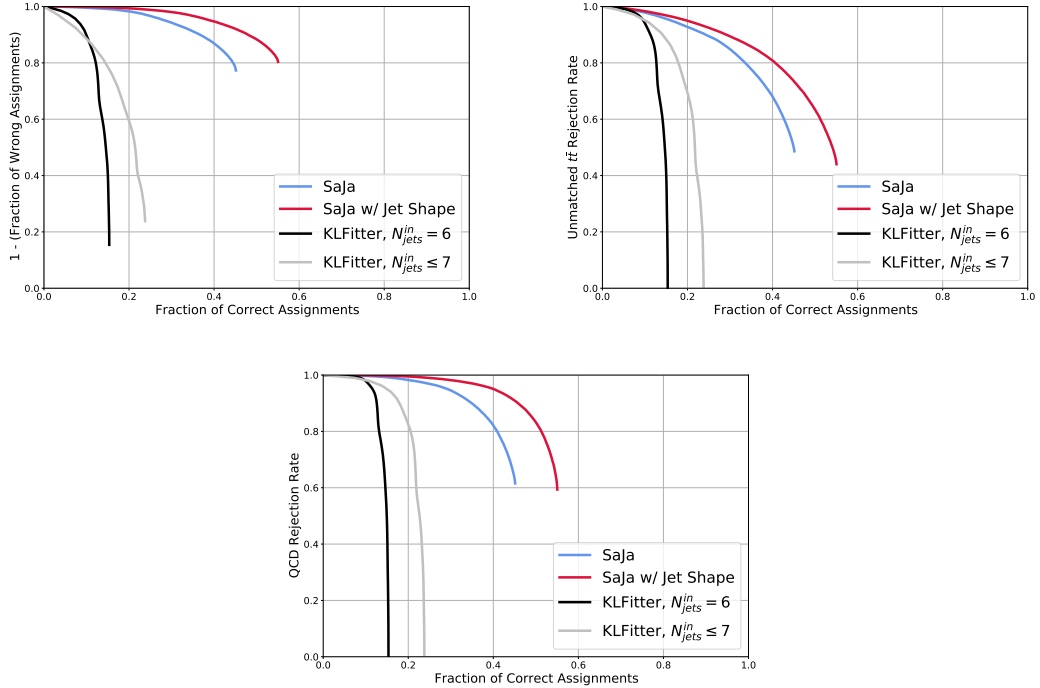


Figure 5: The performance measurement curve. $1 -$ the fraction of wrong assignments for matched $t\bar{t}$ (top left), the unmatched $t\bar{t}$ rejection rate (top right) and QCD multijet rejection rate (bottom) as a function of the fraction of correct assignments for matched $t\bar{t}$. The curves of SAJA without jet shape (blue) and with jet shape (red) are cut short due to the rejection of topologically invalid events.

$t\bar{t}$ by varying the threshold value of the predictive entropy for SAJA or the negative log-likelihood for KLFITTER. The higher the curve is toward the upper right, the better the model performance and the figures show that SAJA exceeds the performance of KLFITTER in all aspects. The curves of SAJA are cut short due to the rejection topologically invalid assignments. The fraction of topologically valid assignments of SAJA on the matched $t\bar{t}$ events, the unmatched $t\bar{t}$ events and QCD multijet events are shown in figure 6. For cases, jet shape information increase the fraction of topologically valid events.

Figure 7 shows the fraction of correct assignments as a function of jet multiplicity. The performance difference between SAJA and KLFITTER are largest in $N_{\text{Jets}} = 7$ or 8, which corresponds to the bulk of the $t\bar{t}$ population that are matched, as shown in figure 3. SAJA is able to better learn the underlying $t\bar{t}$ event topology when given jet shapes. The fraction of topologically valid events for the unmatched $t\bar{t}$ and QCD multijet events also increases, but the increases are relatively small and can be easily rejected by the predictive entropy cut.

Figure 8 shows the reconstructed W and top mass distributions of SAJA with jet shape using the predictive entropy cut of 0.074. The total integrated luminosity of 35.91 fb^{-1} is used for the normalization. Clear peaks can be found in the W and top mass range.

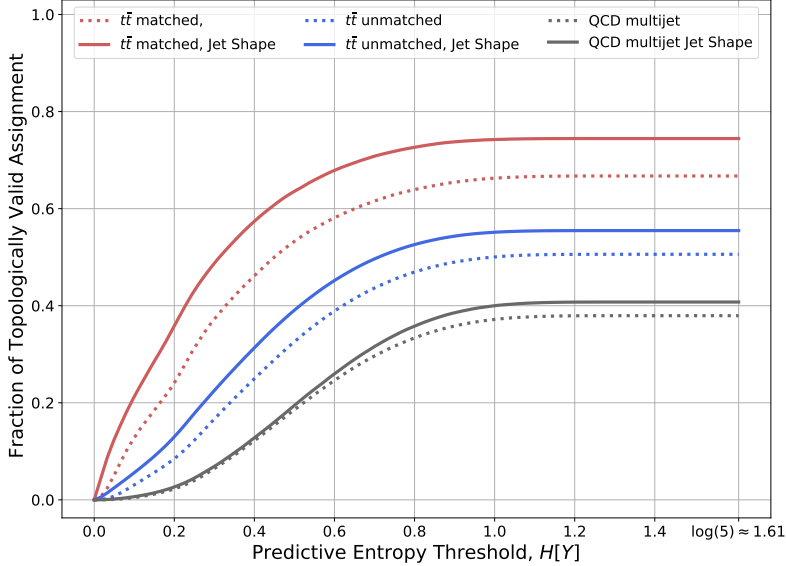


Figure 6: The fraction of topologically valid assignments of SAJA with jet shape (solid) and without jet shape (dotted) as a function of the predictive entropy threshold cut on matched $t\bar{t}$ events (red), unmatched $t\bar{t}$ events (blue), and QCD multijet (black).

Figures 9 shows jet-level normalized confusion matrices for SAJA with and without additional jet shape variables. Jet shape information increases the accuracy of predictions for b-jets and other jets by about 5%.

Figure 10 shows the performance curve for test samples generated using MG5_AMC@NLO interfaced to PYTHIA8, POWHEG interfaced to PYTHIA8 and POWHEG interfaced to HERWIG++. It can be seen from the figure that SAJA without jet shape information is relatively insensitive to which event generator is used. However, SAJA with jet shape information shows a difference in performance, particularly to the parton shower, with the HERWIG++ sample having lower performance than the PYTHIA8 samples.

4.2 Predictive Entropy

Figure 11 shows the predictive entropy distributions of SAJA with and without additional jet shape variables. Correctly assigned $t\bar{t}$ events have lower uncertainty than wrongly assigned $t\bar{t}$, unmatched $t\bar{t}$, or QCD events. As expected, the predictive entropy can be used to effectively veto wrong assignments and background events. For SAJA without jet shape, the second peak near $H[Y] = 0.2$ of correct $t\bar{t}$ assignment distribution is because of events where one or two b-jet is not b-tagged and there are no b-tagged other jets. This undesired second peak is not observed in the case of SAJA with jet shape variables. Also, the peak of the QCD distribution is located at a larger entropy than the other distributions. This means that the predictive entropy of SAJA works well as an out-of-distribution detection method

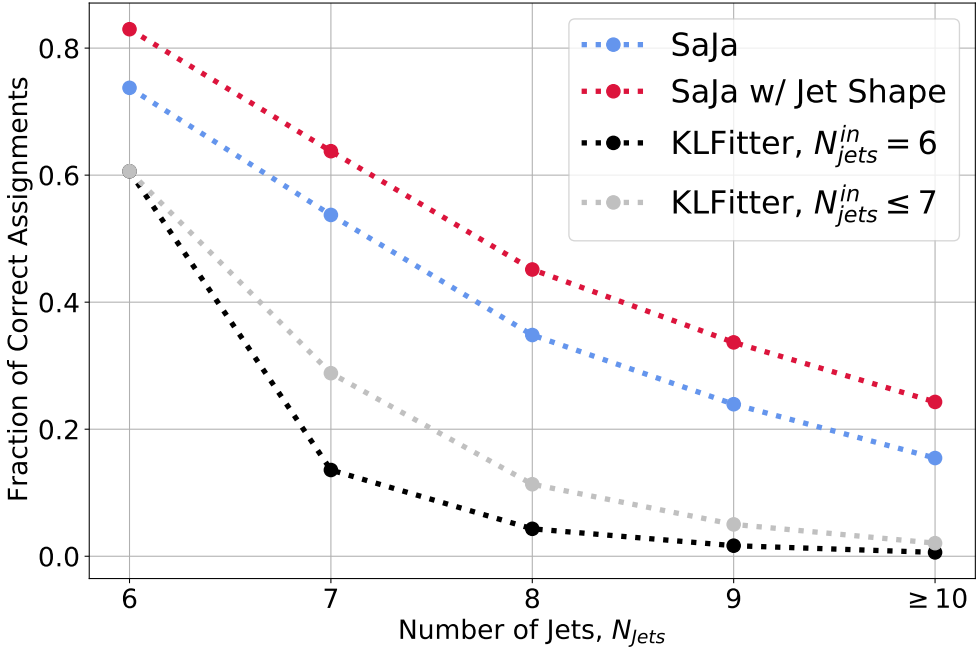


Figure 7: The fraction of correct assignments vs. the jet multiplicity of SAJA without jet shape (blue), SAJA with jet shape (red), KLFITTER with up to 6 jets (black), and KLFITTER with up to 7 jets (gray).

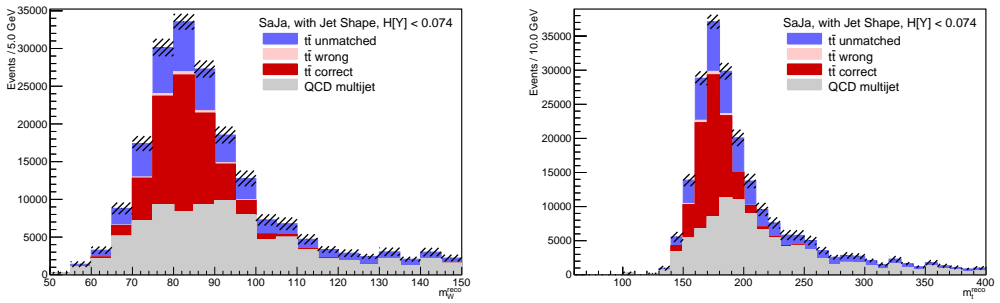


Figure 8: Reconstructed mass distribution of W boson (left) and top quark (right). unmatched $t\bar{t}$ (blue), wrongly assigned $t\bar{t}$ (pink), correctly assigned $t\bar{t}$, and QCD multijet (gray).

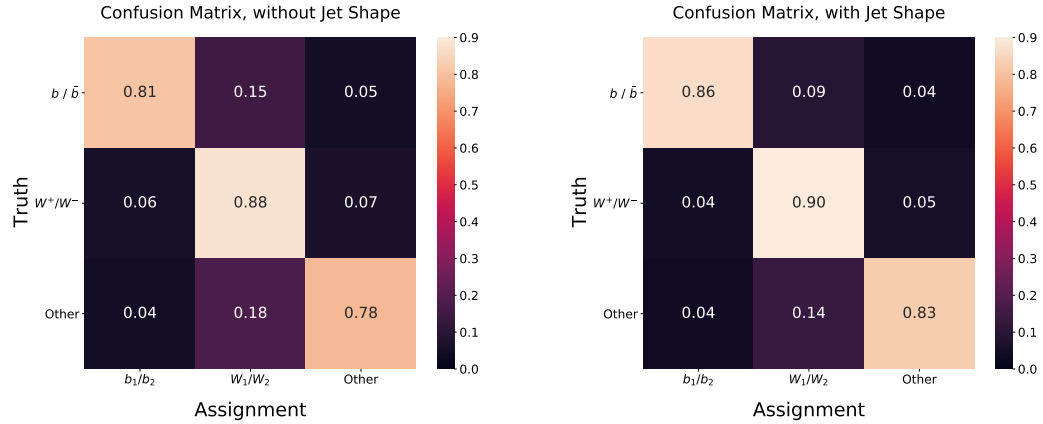


Figure 9: Jet-level normalized confusion matrices for SAJA without jet shape (left) and with jet shape (right). The rows of the matrices correspond to the truth label given by the jet-parton matching and the columns do the prediction of SAJA.

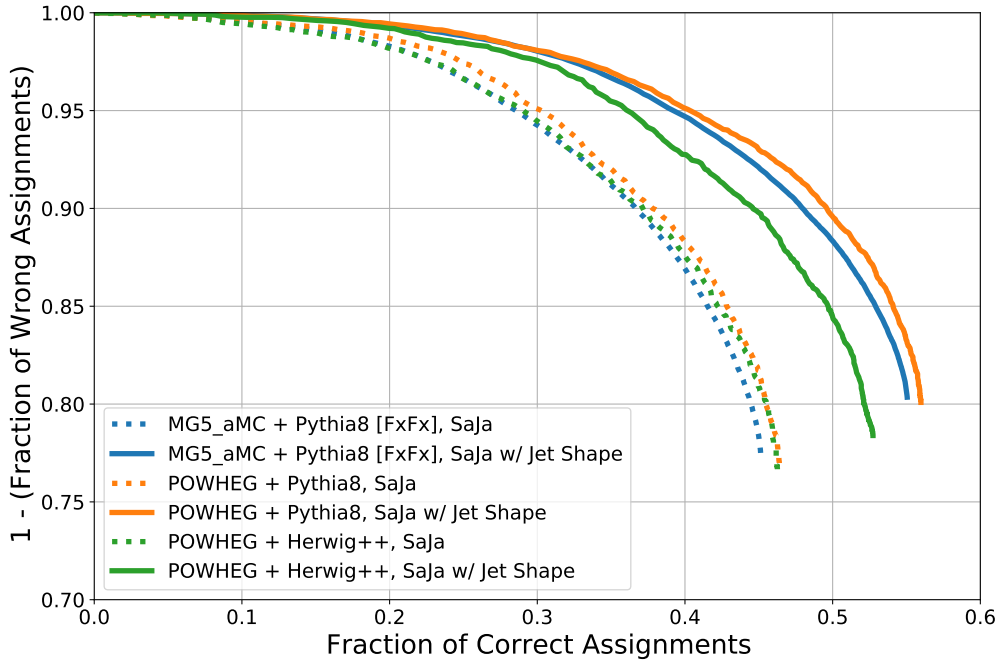


Figure 10: The fraction of wrong assignments as a function of correct assignments for matched $t\bar{t}$ of SAJA, which is trained on MADGRAPH5_AMC@NLO interface to PYTHIA8.

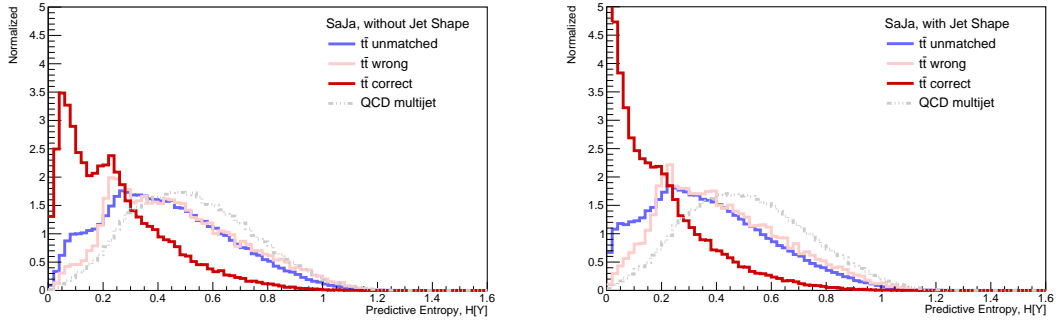


Figure 11: The prediction entropy distribution of (left) SAJA without jet shape and (right) SAJA with jet shape.

without any additional training process or uncertainty calibrations. With an alternative training scheme incorporating the expected SM channels, this method could potentially be used for a model-independent new physics search.

4.3 Model Interpretability

One of the benefit of the attention-based model is that the attention weight matrices shows dependencies between the input elements [6, 9]. Since the model is invariant under the permutation of the jets, it is possible to sort the jets using the jet-parton matching information without loss of generality, for display purposes. Figure 12 shows the average of attention weight matrices block by block for the correct assignment in the matched $t\bar{t}$ events. Rows correspond to queries and columns correspond to keys and so each row is normalized using the softmax function. In the first block, the diagonal elements have the highest values in each row and show strong attention between jets originating from the same top quark. It can therefore be seen that the first block performs the jet representation learning.

The second to fourth blocks show relatively uniform attention weights and seem to perform the event-level representation learning. The fifth and sixth blocks shows strong attention to jets originating from the same top quark again. Also, in the last sixth block, the diagonal component is very small. So, the fifth and sixth blocks extract the information required for the jet-parton assignment.

This model interpretability, enhanced using Monte Carlo information, can be used for the transfer learning of other event properties. For example, we can remove the top two layers and then use SAJA as a pre-trained backbone to speed up the training of full-event classification or for a regression output targeting the kinematics of the reconstructed top.

4.4 Latency

Figure 13 shows the average inference time per event, comparing SAJA and KLFITTER. We used a NVIDIA V100 GPU, and a Intel(R) Xeon(R) CPU E5-2630 v2 @ 2.60GHz CPU. The SAJA network can be processed in batches, allowing for a large speedup, especially on the GPU, while the KLFITTER fits must be performed one at a time, and so have fixed times. The graph shows that even for a batch size of one, the zero-permutation SAJA network is

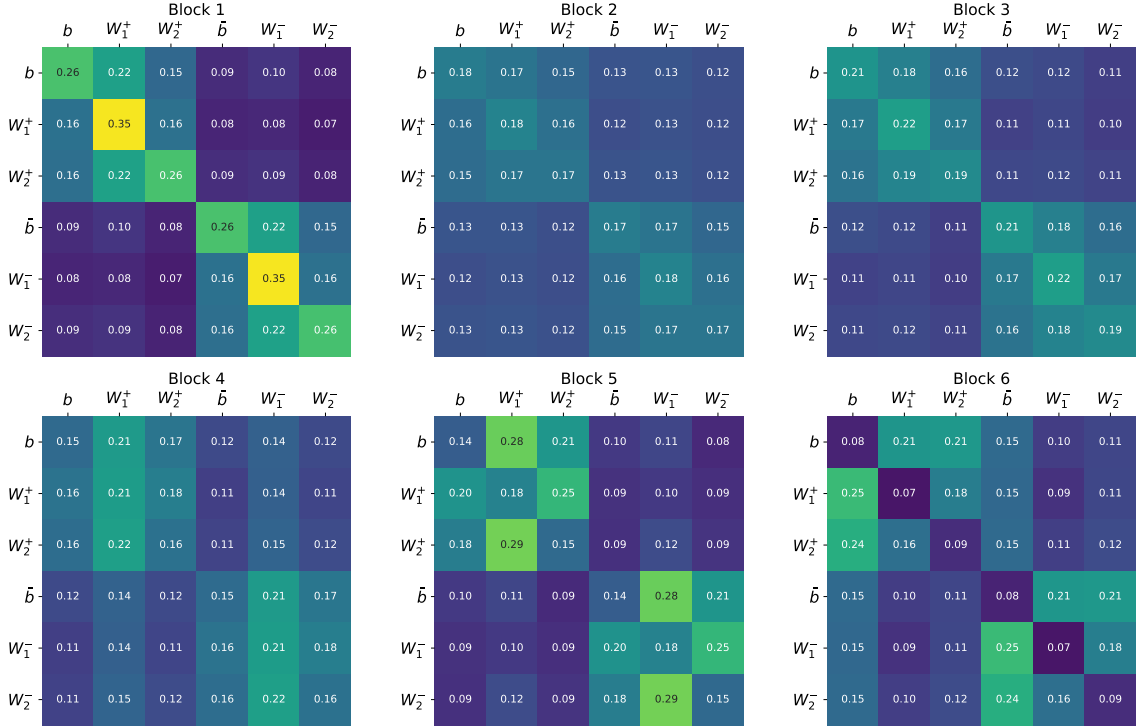


Figure 12: The average of attention matrices block-by-block for the correct assignment in the matched $t\bar{t}$ events. b and \bar{b} are bottom and anti-bottom quarks. W_1^+ is higher p_T of the two quarks, the decay products of W^+ boson.

outperforming KLFITTER, while a two-order-of-magnitude speed up in inference time is possible by fitting in large batches. When SAJA with jet shape takes a batch containing 1000 events of up to 12 jets, the maximum GPU memory allocated for the tensor, which is the model’s parameters and all the inputs, is about 181 MB.

5 Conclusions

In this paper, we introduced the SAJA network for jet-parton assignment in high-energy physics events. SAJA uses self-attention blocks over the jet inputs to calculate probabilities for assignments using only jet position invariant linear transformations and without requiring jet permutations. We introduced a new objective function to train the SAJA network on jet-parton assignment for fully-hadronic top pair events. SAJA performed better and faster than the traditional kinematic likelihood methods, as implemented in KLFITTER. In particular, the inference time for SAJA was two orders of magnitude faster than the time for KLFITTER, even when KLFITTER is restricted to use only 6 jets, while SAJA is unrestricted. The SAJA network shows great potential for future use, as it could be easily adapted to other topologies of arbitrary complexity, such as fully-hadronic $t\bar{t}H$, for which traditional machine learning techniques have been computationally infeasible. This also

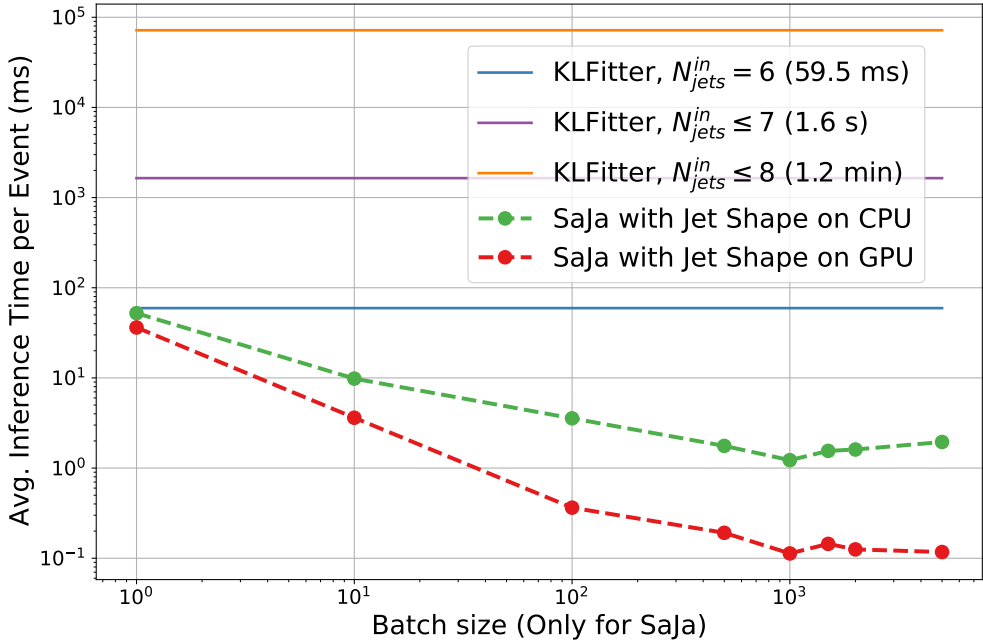


Figure 13: The average inference time per events.

has potential to be used at the trigger level, where speed is of upmost importance.

Acknowledgments

This article was supported by the computing resources of the Global Science Experimental Data Hub Center (GSDC) at the Korea Institute of Science and Technology Information (KISTI). J.L. and S.Y. are supported by the National Research Foundation of Korea (NRF) grant funded by the Korea government (MSIT) (2019R1C1C1009200). I.W. is supported by the Korea Research Fellowship Program through the NRF funded by the Ministry of Science and ICT (2017H1D3A1A01052807). I.P. is supported by the Basic Science Research Program through the NRF funded by the Ministry of Education (2018R1A6A1A06024977).

References

- [1] CMS Collaboration, *Measurement of the top quark mass in the all-jets final state at $\sqrt{s} = 13$ TeV and combination with the lepton+jets channel*, *Eur. Phys. J. C* **79** (2019) 313, [[arXiv:1812.10534](https://arxiv.org/abs/1812.10534)].
- [2] ATLAS Collaboration, *Measurement of the top-quark mass in the fully hadronic decay channel from ATLAS data at $\sqrt{s} = 7$ TeV*, *Eur. Phys. J. C* **75**, 158 (2015), [[arXiv:1409.0832](https://arxiv.org/abs/1409.0832)]

- [3] J. Erdmann, S. Guindon, K. Kroeninger, B. Lemmer, O. Nackenhorst, A. Quadt and P. Stolte, *A likelihood-based reconstruction algorithm for top-quark pairs and the KLFitter framework*, *Nucl.Instrum.Meth.* **748** (2014) 18 , [[arXiv:1312.5595](#)].
- [4] M. Erdmann, B. Fischer and M. Rieger, *Jet-parton assignment in ttH events using deep learning*, *JINST* **12** (2017) P08020, [[arXiv:1706.01117](#)].
- [5] J. Erdmann, T. Kallage, K. Kröninger and O. Nackenhorst, *From the Bottom to the Top-Reconstruction of t̄t Events with Deep Learning*, *JINST* **14** (2019) P11015, [[arXiv:1907.11181](#)]
- [6] D. Bahdanau, K. Cho, Y. Bengio *Neural machine translation by jointly learning to align and translate*, [[arXiv:1409.0473](#)].
- [7] A.P Parikh, O. Täckström, and D. Das and J. Uszkoreit, *A decomposable attention model for natural language inference*, [[arXiv:1606.01933](#)].
- [8] D. Britz, A. Goldie, M.T. Luong and Q. V Le *Massive exploration of neural machine translation architectures*, [[arXiv:1703.03906](#)]
- [9] A. Vaswani, N. Shazeer, N. Parmar, J. Uszkoreit, L. Jones, A. N. Gomez, Ł. Kaiser, and I. Polosukhin, *Attention is all you need*, in the proceedings of *Neural Information Processing Systems* (NIPS 2017), December 4-9, Long Beach, U.S.A. (2017), [[arXiv:1706.03762](#)].
- [10] D. Amodei, C. Olah, J. Steinhardt, P. Christiano, J. Schulman, and D. Mané, *Concrete problems in AI safety*, [[arXiv:1606.06565](#)]
- [11] Y. Gal, *Uncertainty in deep learning*, University of Cambridge (2016).
- [12] C. Guo, G. Pleiss, Y. Sun, and K. Q. Weinberger, *On calibration of modern neural networks*, [[arXiv:1706.04599](#)]
- [13] J. Alwall, M. Herquet, F. Maltoni, O. Mattelaer and T. Stelzer, *MadGraph 5 : Going Beyond*, *JHEP* **06** (2011) 128, [[arXiv:1106.0522](#)].
- [14] T. Sjöstrand et al., *An introduction to PYTHIA 8.2*, *Comput. Phys. Commun.* **191** (2015) 159 [[arXiv:1410.3012](#)]
- [15] The DELPHES 3 collaboration, *DELPHES 3: a modular framework for fast simulation of a generic collider experiment*, *JHEP* **02** (2014) 057 [[arXiv:1307.6346](#)].
- [16] M. Cacciari, G. P. Salam and G. Soyez, *FastJet user manual*, *Eur. Phys. J. C* **72** (2012) 1896, [[arXiv:1111.6097](#)].
- [17] S. Alioli, P. Nason, C. Oleari, and E. Re, *A general framework for implementing NLO calculations in shower Monte Carlo programs: the POWHEG BOX*, *JHEP* **06** (2010) 043, [[arXiv:1002.2581](#)]
- [18] S. Frixione, P. Nason, and C. Oleari, *Matching NLO QCD computations with Parton Shower simulations: the POWHEG method*, *JHEP* **11** (2007) 070 [[arXiv:0709.2092](#)]
- [19] P. Nason, *A New method for combining NLO QCD with shower Monte Carlo algorithms*, *JHEP* **11** (2004) 040 [[arXiv:hep-ph/0409146](#)]
- [20] S. Frixione, P. Nason, and G. Ridolfi, *A Positive-weight next-to-leading-order Monte Carlo for heavy flavour hadroproduction*, *JHEP* **09** (2007) 126 [[arXiv:0707.3088](#)]
- [21] M. Bähr et al., *Herwig++ physics and manual*, *Eur. Phys. J. C* **58** (2008) 639, [[arXiv:0803.0883](#)].

- [22] A. L. Maas, A. Y. Hannun and A. Y. Ng, *Rectifier nonlinearities improve neural network acoustic models*, in *Proceedings of the 30 th International Conference on Machine Learning*, Atlanta, Georgia, USA, 2013.
- [23] G. E. Hinton, N. Srivastava, A. Krizhevsky, I. Sutskever and R. R. Salakhutdinov, *Improving neural networks by preventing co-adaptation of feature detectors* [[arXiv:1207.0580](https://arxiv.org/abs/1207.0580)].
- [24] Ba, Jimmy Lei and Kiros, Jamie Ryan and Hinton, Geoffrey E, *Layer normalization*, [[arXiv:1607.06450](https://arxiv.org/abs/1607.06450)].
- [25] K. He, X. Zhang, S. Ren, and J. Sun, *Deep residual learning for image recognition*, in the proceedings of the *IEEE conference on computer vision and pattern recognition (CVPR 2016)*, June 27-30, Las Vegas, NV, USA (2016), [[arXiv:1512.03385](https://arxiv.org/abs/1512.03385)]
- [26] T. Cornelis, *Quark-gluon jet discrimination at CMS*, in Proceedings of the second annual conference on Large Hadron Collider Physics (LHCP), Columbia University, New York City, U.S.A. June 2-7, 2014, [[arXiv:1409.3072](https://arxiv.org/abs/1409.3072)].
- [27] J. S. H. Lee, I. Park, I. J. Watson, and S. Yang, *Quark-Gluon Jet Discrimination Using Convolutional Neural Networks*, *J. Korean Phys. Soc.* **74**, 219–223 (2019).
- [28] D. P. Kingma and J. Ba, *Adam: A method for stochastic optimization* [[arXiv:1412.6980](https://arxiv.org/abs/1412.6980)].
- [29] A. Paszke et al., *PyTorch: An Imperative Style, High-Performance Deep Learning Library*, in *Proceedings of Advances in Neural Information Processing Systems (NeurIPS 2019)*, December 8-14, Vancouver Convention Center, Canada (2019), [[arXiv:1912.01703](https://arxiv.org/abs/1912.01703)]